Chemical Physics 523 (2019) 198–204

Contents lists available at ScienceDirect

Chemical Physics

journal homepage: www.elsevier.com/locate/chemphys

A simple method to fabricate metal doped TiO_2 nanotubes

Aijo John K.[a,*], Johns Naduvath[b], Stephen K. Remillard[c], Sadasivan Shaji[d], Paul A. DeYoung[c], Zachary T. Kellner[c], Sudhanshu Mallick[e], Manju Thankamoniamma[f], Gunadhor S. Okram[g], Rachel Reena Philip[a,*]

[a] Department of Physics, Union Christian College, Aluva, Kerala, India
[b] Department of Physics, St. Thomas College (Autonomous), Thrissur, Kerala, India
[c] Department of Physics, Hope College, Holland, MI 49423, USA
[d] Autonomous University of Nuevo León, Facultad de IngenieríaMecánica y Eléctrica, Mexico
[e] Department Of Metallurgical Engineering and Material Science, Indian Institute of Technology, Mumbai, Maharashtra, India
[f] Department of Physics, Sree Sankara College, Kalady, Kerala, India
[g] UGC DAE Consortium for Scientific Research, Indore, M. P, India

ARTICLE INFO

Keywords:
Titanium dioxide
Nanotubes
Doping

ABSTRACT

A simple electrochemical method for effective doping of TiO_2 nanotubes with metals is presented here. The doping is done in a two-stage cost effective process and is found to result in uniform doping concentration, without any surface layer formation, in the nanotubes. Detailed structural, compositional, optical and electrical analyses are done on the nanotubes doped with copper metal. The cu metal doping is found to produce tuning of the electrical and optical properties. The doped tubes with increased conductivity are better suited in dye sensitized solar cells (dsscs) whereas enhanced visible light absorbing capacity makes them better candidates for photocatalytic applications. Further the success of this method in doping TiO_2 nanotubes with any metal of choice is demonstrated by testing aluminum metal doping in the nanotubes.

1. Introduction

Titanium dioxide is a versatile wide bandgap semiconducting metal oxide, which has undergone immense research studies in the past decade on account of the wide bandgap and band edge positions suitable for photochemical and photo catalytic applications [1–3]. Even though the large band gap of TiO_2 (~3 eV) is desirable for several applications, this property creates a performance barrier in the sun driven applications since only the ultra violet part of the solar spectrum can be absorbed and utilized by TiO_2. Reports indicate that the poor response of TiO_2 to the visible part of the solar radiation limits its photocatalytic applications whereas the low electrical conductivity adversely affects its use in optoelectronic devices [4–11]. An improvement in the electrical conductivity of the TiO_2 is very much relevant in applications such as dye sensitized solar cells (DSSCs), in which the titanium dioxide nanomaterials are used as electron transport pathways [12]. In DSSC, the photo excited electrons are injected into the conduction band of the titanium dioxide nanomaterials serving as electrodes and are transported to the back metal contact [4].

Improving the optical and electrical properties of the Titanium dioxide nanomaterials by doping, band gap engineering, and sensitization is a keen field of research today [13,14]. The lower level of the conduction band of the titanium dioxide is formed by Ti 3d states, while the upper level of the valence band is formed by O 2p levels. Thus, the modification of the band gap can be done by shifting the valence and conduction bands and by introduction of localized states in the band gap. But very few studies on tuning the band gap of Titanium dioxide nanotubes (TONTs) are found in literature [15,16]. This paper presents doping as an effective means of bandgap tailoring of TONTs.

Several doping methods such a high energy ion implantation, co-sputtering, annealing in dopant gas atmosphere and use of alloys have been used to modify the optoelectronic properties of titanium dioxide nanomaterials [13]. Most of these doping processes are done on a very high energy budget. Cost effective methods for metal doping of TONTs is particularly important. Here we introduce a simple two-electrode electrochemical doping method for fabricating metal doped TiO_2 nanotubes, which can modify the optical and electronic properties of the titanium dioxide nanotubes at a lower energy budget. In this paper, a novel method for metal doping of TiO_2 nanotubes and an analysis of the structural, compositional, electrical and optical properties of Cu (I

* Corresponding author.
E-mail address: reenatara@gmail.com (R.R. Philip).

https://doi.org/10.1016/j.chemphys.2019.04.028
Received 12 December 2018; Received in revised form 6 April 2019; Accepted 27 April 2019
Available online 29 April 2019
0301-0104/

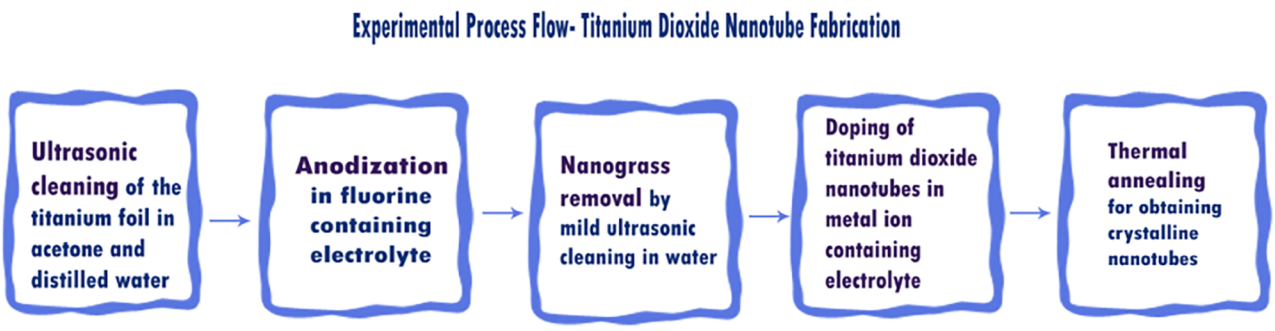

Fig. 1. Process flow of the metal doping of TiO_2 nanotubes.

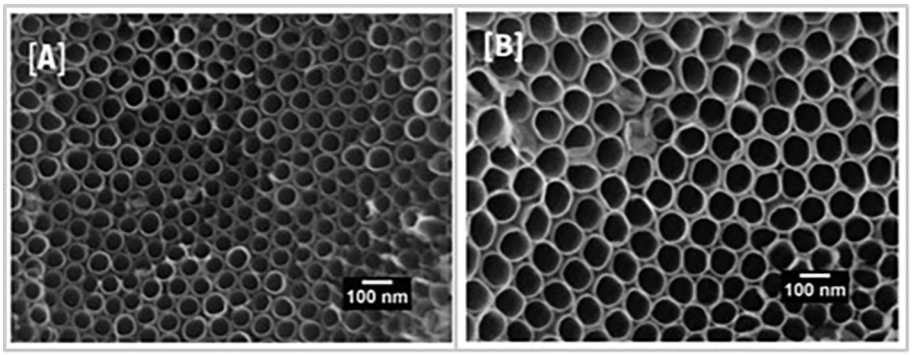

Fig. 2. SEM images of the undoped (A) and copper metal doped (B) of TiO_2 nanotubes.

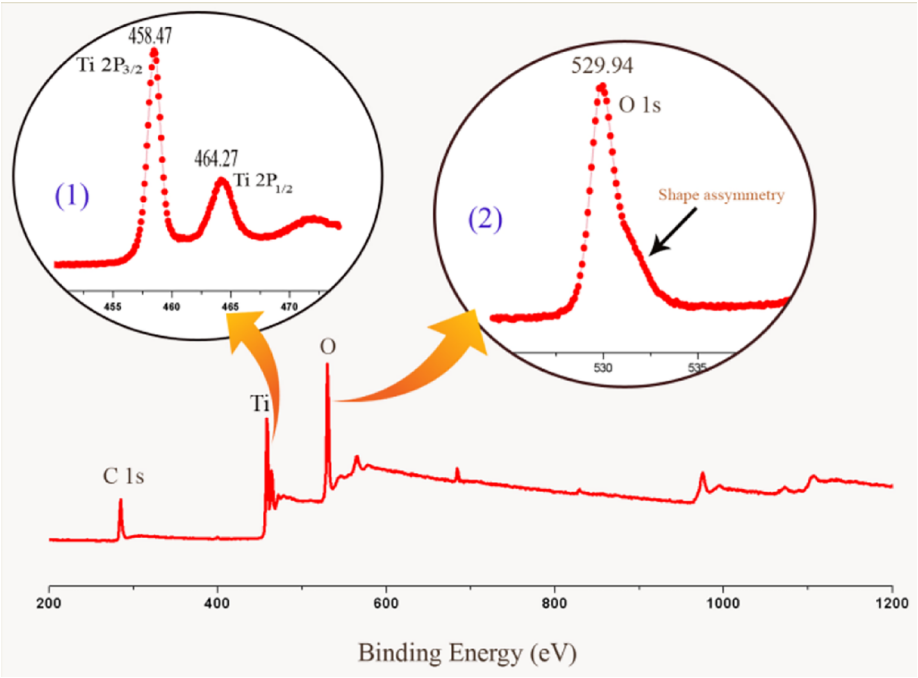

Fig. 3. XPS of pure TONTs. Detailed spectra of Titanium [Inset 1], detailed spectra of Oxygen [Inset 2].

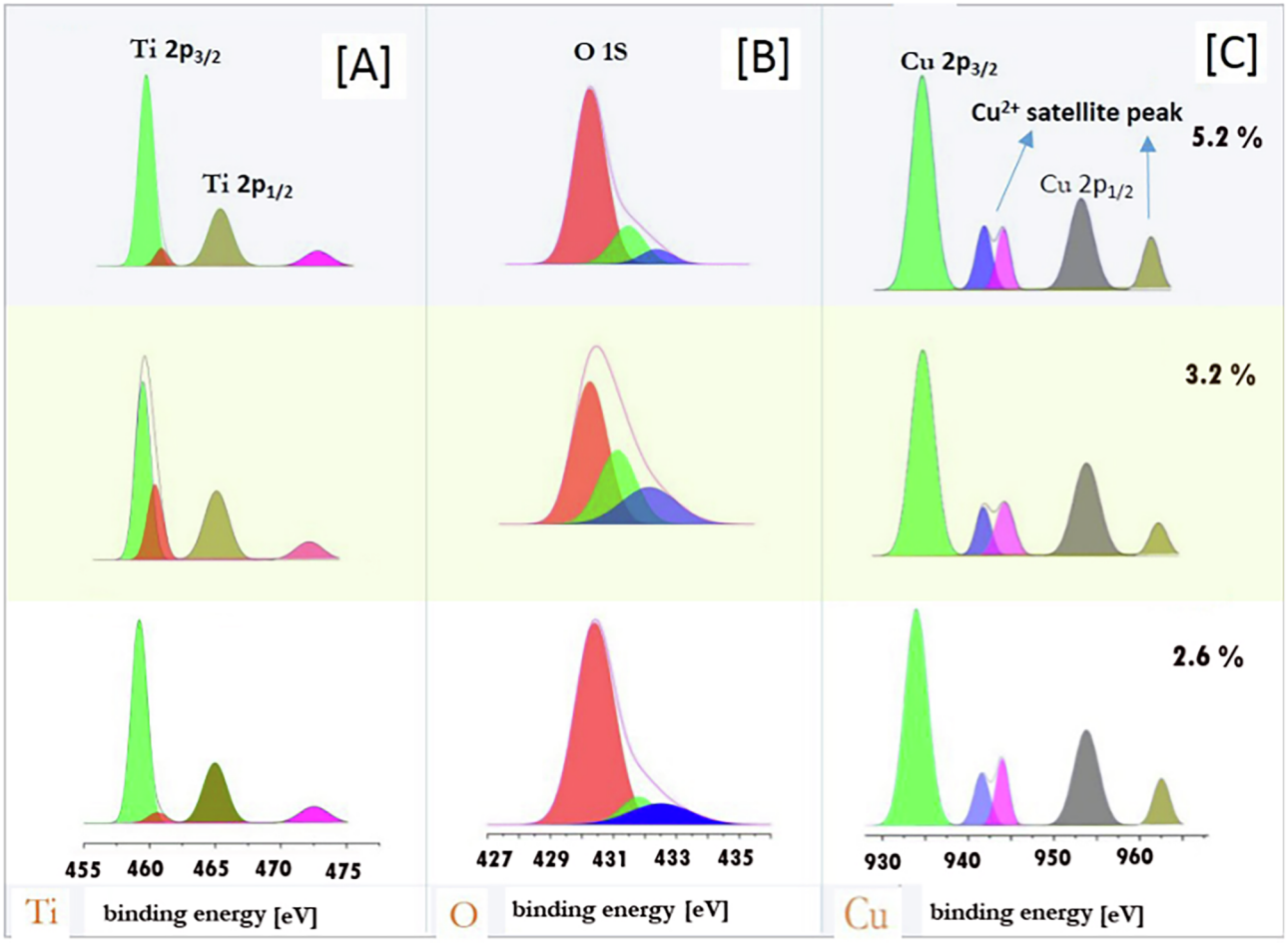

Fig. 4. Detailed XPS spectra of doped samples [A] Titanium [B] Oxygen [C] Copper.

Table 1
Shift in Titanium peaks after copper doping.

Cu doping %	Shift in $Ti2P_{3/2}$	Shift in $Ti2P_{1/2}$
2.6	0.76 eV	0.74 eV
3.2	0.90 eV	0.85 eV
5.2	1.04 eV	0.91 eV

Group element) doped TONTS fabricated by this method is presented in detail and then the suitability of the method in doping other metals is tested by attempting doping with the III group metal Al.

2. Experimental methods

The electrochemical synthesis of metal doped TONTs is done by a two-step method. Well aligned titanium dioxide nanotubes are fabricated by the conventional electrochemical anodization process [3]. The process flow for the metal doping is shown in Fig. 1. Ultrasonically cleaned titanium foils are anodized in a fluorine containing electrolyte. These nanotubes are used for copper metal doping in a two electrode system after removing the surface deposited nanograss. Doping is done in 1 Molar solution of copper sulphate electrolyte using TONTs as cathode and platinum as anode. Metal doping is done by applying a voltage between anode and cathode. The process is done for different voltage durations (5, 10 and 20 s) for achieving doped nanotubes with different doping concentrations. The as-fabricated copper doped nanotubes are thermally annealed for attaining perfectly crystalline copper doped TONTs.

The morphological analysis of the doped titanium dioxide nanotubes is characterized by Field Emission Scanning Electron Microscope (FEG-SEM). Compositional analysis is done using Rutherford Backscattering Spectroscopy (RBS) and X-ray photoelectron spectroscopy (XPS). The structural properties are analysed using X-ray diffraction (XRD). Further, the conductivity measurements and diffuse reflectance spectrum are recorded for the electrical and optical studies.

3. Results and discussion

Fig. 2 shows the surface SEM images of the undoped [A] and copper doped [B] TONTs. These nanotubes show an approximate diameter of 80 nm and an approximate wall thickness 15 nm. It is essential to maintain the tubular structure of the TONTs even after the doping. The SEM image shows that copper doping of the titanium dioxide nanotubes is done without destroying the porous nature of the nanotubes. No copper metal layer is present at the top of the TONTs. This suggests the doping of copper into the nanotubular walls. Ionic radius of copper and titanium is comparable which allows incorporation of copper into TiO_2 framework.

The stoichiometry of the as-anodized nanotubes (anodized in 0.5 wt % ammonium fluoride and 2 vol% water in ethylene glycol electrolyte,

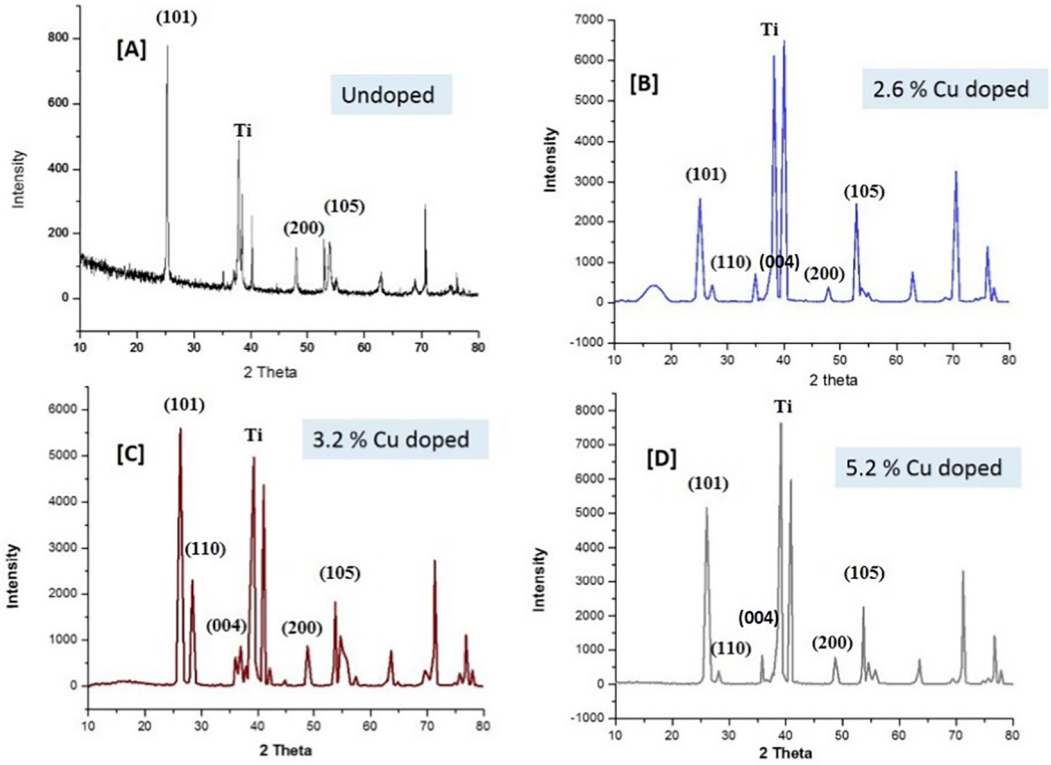

Fig. 5. XRD pattern of undoped TONTs and copper doped TONTs [A] undoped [B] 2.6% copper doped [C] 3.2% copper doped [D] 5.2% copper doped.

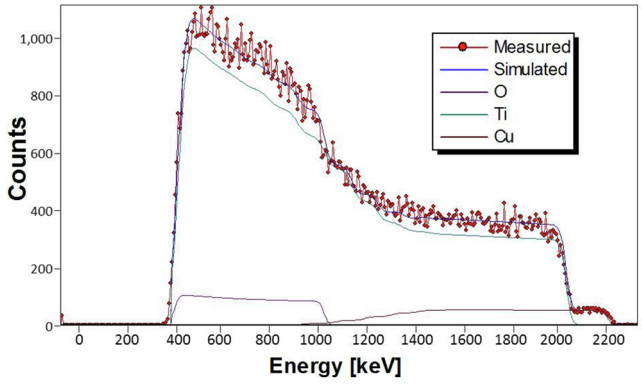

Fig. 6. RBS spectra of pattern 2.6% copper doped TONTs.

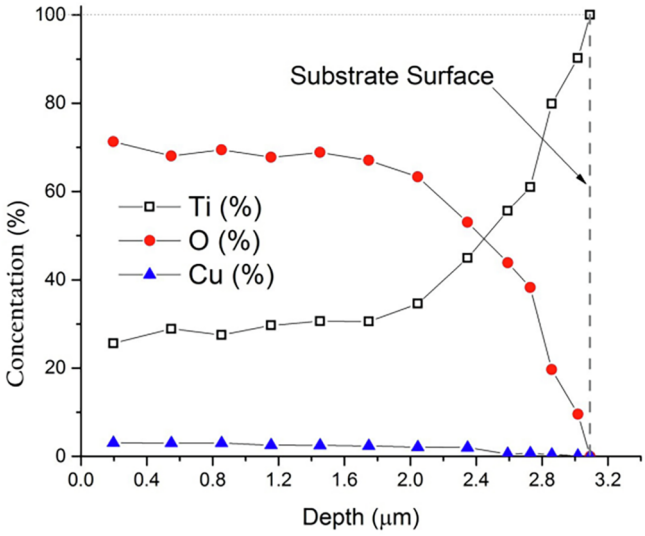

Fig. 7. RBS depth and concentration profile of 2.6% copper doped TONTs.

50 V- 60 min) is analysed using a spectrometer fitted with Mg and Al twin anode (VSW Scientific Instruments) X-Ray Photoelectron Spectroscopy (XPS). Fig. 3 shows the XPS of the as-prepared TONTs. The anodized films are composed of Titanium (2p), Oxygen (1s), Fluorine (1s) and Carbon (1s) peaks.

The XPS detailed spectra of titanium and oxygen in TONTs are given in the insets of the Fig. 3. The peaks observed at 458.47 eV and 464.27 eV can be attributed to the Ti $2P_{3/2}$ and Ti $2P_{1/2}$. Oxidation state of the titanium can be found as +4 which indicates the formation of the TiO_2. The Oxygen 1s peak is observed at 529.94 eV. There is a shape asymmetry in the oxygen peak towards the higher binding energy which can be due to the contributions from different bonding of the oxygen atoms such as from the presence of surface hydroxyl ions and organic contaminants [17]. For analysing the successful doping of copper into titanium dioxide nanotubes and chemical states of Cu, Ti and O, X-ray photoelectron spectroscopy analysis of the copper doped TONTs (Fig. 4) is done. Fig. 4c shows the XPS detailed spectra of the Cu doped TONTs. The XPS analysis of the doped samples shows the presence of copper in all the doped samples. The copper dopedTONTs show a dopant concentration of 2.6, 3.2 and 5.2% respectively for doping times of 5 s, 10 s and 20 s.

The detailed XPS spectra of Titanium, Oxygen and Copper of the copper doped TONTs are shown in Fig. 4 The copper peaks Cu $2p_{3/2}$ and

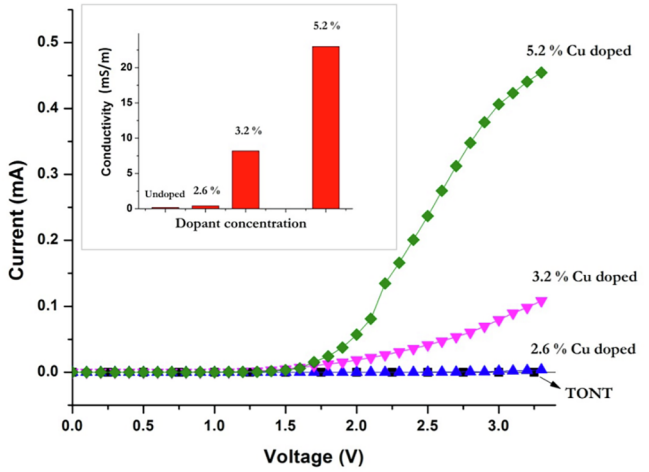

Fig. 8. V-I Characteristics and conductivity of the undoped and copper doped TONTs.

Cu $2p_{1/2}$ for the 2.6% doped TONT are observed at 933.84 and 953.79 eV respectively. In addition, two Cu2+ satellite peaks are present at 942.31 and 962.71 eV. These satellite peaks denote the bonding between Cu and O in the doped samples. Shifts of Ti $2P_{1/2}$ and Ti $2P_{3/2}$ peaks towards the higher binding energy (Shown in Table 1) in the doped samples compared to the pure TONTs can be attributed to the successful doping of the copper into TONTs. The shift in titanium peaks increases systematically as the doping concentration increases.

Fig. 5 depicts the XRD pattern of the undoped (Fig. 5A) and doped nanotubes (Fig. 5B, C, D). Anatase phase of the TiO_2 is present in undoped TONTs with crystal planes (1 0 1), (0 0 4), (2 0 0), (1 0 5) and (1 1 6). The major crystal orientation is along (1 0 1). The crystallinity is found to be increased in Copper doped nanotubes with the major orientation still along (1 0 1) plane and no major change is observed in the structural characteristics of the nanotubes after doping though a small rutile peak belonging to (1 1 0) orientation appears.

The intensity (1 0 1) increases in the copper doped TONTs and the preferential orientation increases with increase in doping concentration, which is suitable for faster carrier transport pathways in optoelectronic devices.

The concentration of the atoms and depth analysis of the copper doped TONTs are analysed using Rutherford Backscattering Spectroscopy (RBS) with 2.97 MeV alpha particles backscattered at 168.2 degrees. This technique depends on the backscattering of the alpha particles from atoms in the sample and element concentration is the main factor determining the backscattering ratios. The layered structure is studied here using RBS analysis, which reveals the doping concentration of copper in the 5 s copper doped nanotubes. Fig. 6 shows the measured and simulated RBS spectrum of copper doped TONTs. The RBS spectrum shows two layers, a top TiO_2 layer in which copper is doped and a bottom titanium metal layer with infinite thickness.

The copper percentage present in the top TiO_2 layer calculated using SIMNRA [18] is 2.9%, which is well in agreement with the XPS results.

Generally, it is difficult to achieve uniform doping using electrochemical methods. Keeping this in view, the depth analysis of the doped samples is performed to study the uniformity of copper doping. The length of the tubes is found in SEM exam to be 3.4 μm. Initial analysis of

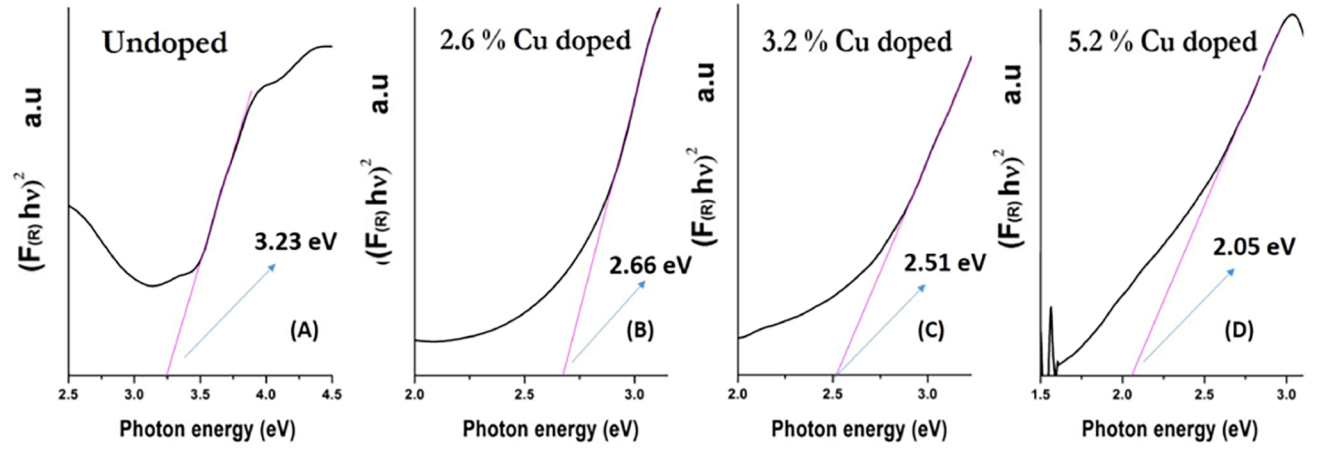

Fig. 9. Kubelka- Munk plots of the undoped and copper doped TONTs.

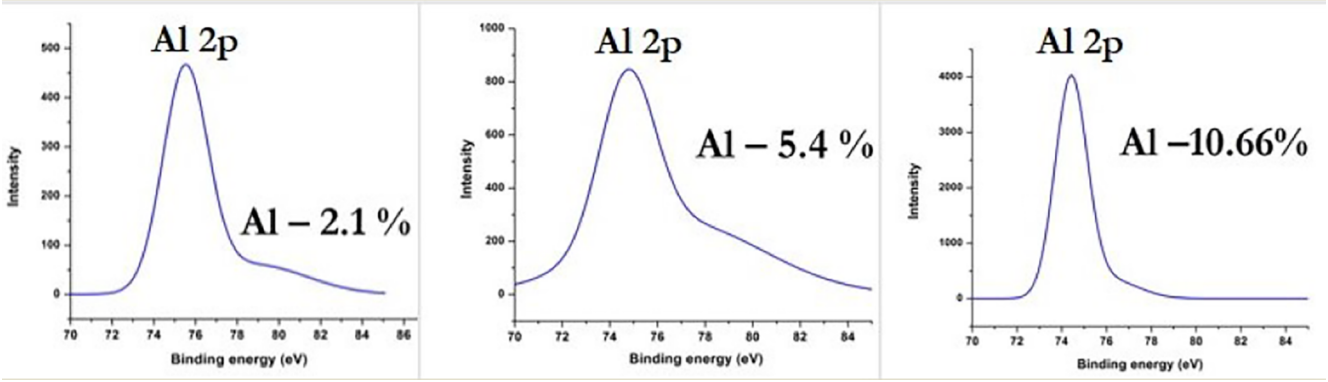

Fig. 10. Detailed XPS scan of the aluminum doped TONTs.

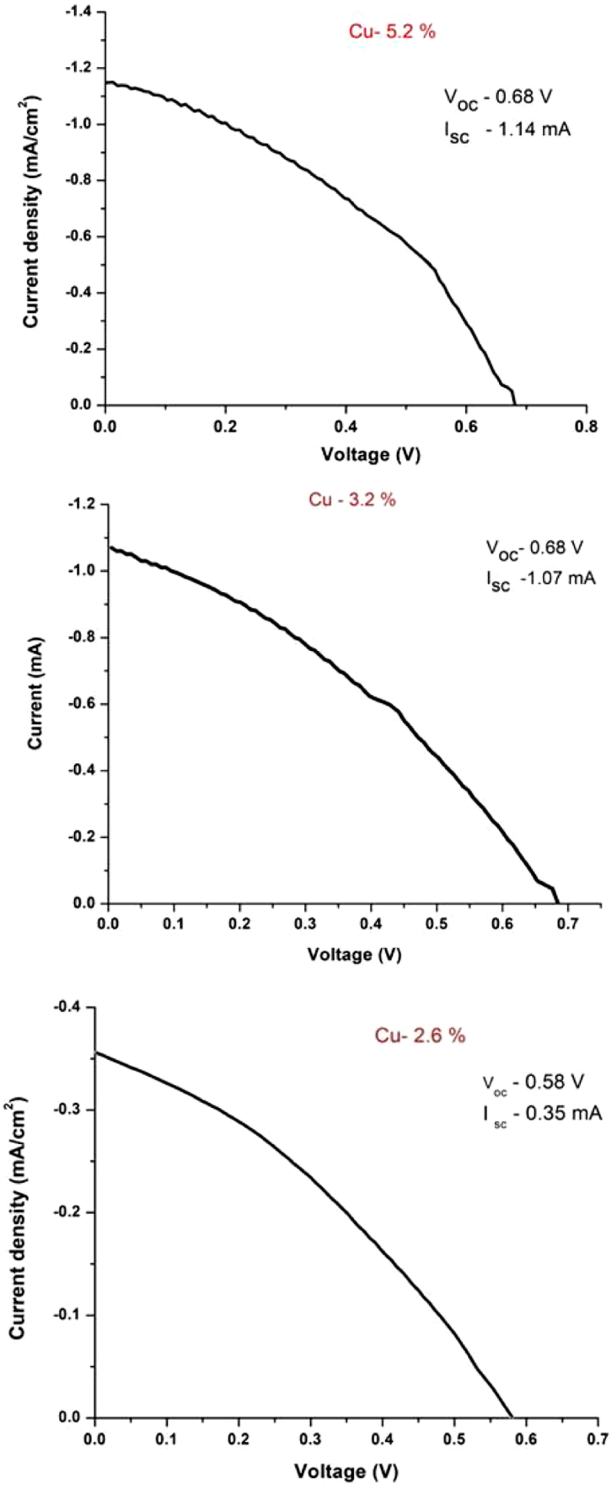

Fig. 11. I–V characteristics of dye sensitized solar cell fabricated using as prepared and Cu doped TONTs.

the RBS results suggests that the TiO_2 is only 1.5 μm thick. However, with an 80 nm diameter and a 15 nm wall thickness, the fill factor of the film is about 41%, which closely corresponds to the discrepancy in depth determinations. The RBS depth analysis of the 5 s copper doped TONT, including the 41% fill factor, is given in Fig. 7.

RBS depth analysis reveals that uniform dopant percentage is up to 3 μm from the surface of the 5 s doped sample. Thereafter uniformity of the doping is lost and the copper percentage decreases near the titanium substrate surface. It is evident from the concentration analysis of the titanium and oxygen that the oxidation of the titanium decreases towards the substrate surface as expected. The analysis shows that Cu is uniformly distributed throughout the entire nanotube and is not simply forming a surface layer near the top of the tubes.

Current- Voltage characteristics are measured in order to compare the charge transport properties of the undoped and doped TONTs. The V-I measurements are done between a top silver electrode and bottom titanium metal electrode. As mentioned earlier, while considering DSSC applications, the poor conductivity ($\sim 10^{-4}$ S/m) of TONT is a limiting factor. It is clear from Fig. 7 that Cu doping is effective in improving the conductivity of TONT. The conductivity increases as the doping percentage increases. While 2.6% doped TONTs show only very small increase in the conductivity, other TONTs with higher doping percentages show drastic change in electrical conductivity. It is interesting to note that the Cu doped TONTs with 5.2% doping show around 2 order magnitude enhanced conductivity when compared to the undoped. The nonlinear behavior of the V-I characteristics may be due to the formation of a Schottky junction between TONT and Ti substrate [19].

The diffuse reflectance spectroscopic analysis of the doped and undoped TONTs reveals that there is a decrease in bandgap as the doping percentage increases (Fig. 8). The bandgap is calculated using Kubleka- Munk plots [20]. The bandgap for undoped TONTs is 3.23 eV, which decreases to 2.66 eV, 2.51 eV, and 2.05 eV as doping concentration increases. This red shift in band gap may be due to the introduction of dopant localized states near the conduction band. This large shift in band gap towards the visible region of the electromagnetic spectrum is of real importance in its application in photocatalysis. (See Fig. 9).

In order to check the applicability of the electrochemical metal doping method to different metals, Aluminium metal doping is attempted by the same process. For this, a 1 M solution of aluminium sulphate is used as the electrolyte. Here also platinum and pure TONTs are used as anode and cathode respectively. Doping is done by applying 50 V between cathode and anode for 5 s, 10 s, and 20 s. The doped samples so obtained are compositionally analysed using XPS (Fig. 10) to confirm the Al doping.

Fig. 10 shows the detailed XPS scan spectra of the aluminium doped TONTs. Al doping for different doping durations of 5 s, 10 s and 20 s are found to result in a doping concentration of 2.1, 5.4 and 10.66% respectively. Al 2p peak positions are present at 74.8 eV. Doping percentage of aluminum is higher compared to copper for the same doping duration, which may be due to the stronger attraction of aluminum ions, possessing an oxidation state +3, towards the cathode.

Further the applicability of the Copper doped nanotubes in dye sensitized solar cells is analysed. The performance of the DSSCs fabricated using as fabricated and copper doped TiO_2 nanoubes is compared. The I-V characteristics is shown in the Fig. 11

The short circuit current increases from 0.35 mA to 1.14 mA as the doping percentage increases from 2.6 to 5.2 and open circuit voltage increases from 0.58 V to 0.68 V (Table 2). The increase in the short circuit current may be due to the increase in the nanotubular conductivity through doping. The efficiency of the solar cell also increases with the doping concentration.

4. Conclusions

In succinct, this paper reports development of a facile electrochemical cost effective method for effective metal doping of the TiO_2 nanotubes which can be applied to all metal dopants. This two-stage method has succeeded in producing uniform doped nanotubes fortuning of optoelectronic properties.

Table 2
Solar cell parameters of the dye sensitized solar cell fabricated using as prepared and Cu doped TONTs.

Sample description	Isc (mA)	Voc (V)	Fill factor	Efficiency (%)
2.6 % Cu doped	0.35	0.58	0.49	0.11
3.2 % Cu doped	1.07	0.68	0.38	0.25
5.2 % Cu doped	1.15	0.68	0.38	0.30

Acknowledgement

AJK, RRP and MT acknowledge UGC-DAE, Indore for the funding through a collaborative research scheme (CRS) CSR-IC/CRS-94/2014-15/600. MT acknowledges DST Govt. of India- FIST Scheme – 487/DST/FIST/15-16.

References

[1] J.M. Macak, H. Tsuchiya, A. Ghicov, K. Yasuda, R. Hahn, S. Bauer, P. Schmuki, Curr. Opin. Solid State Mater. Sci. 11 (2007) 3.
[2] D. Regonini, C.R. Bowen, A. Jaroenworaluck, R. Stevens, Mater. Sci. Eng.: R: Rep. 74 (12) (2013) 377.
[3] P. Roy, S. Berger, P. Schumuki, Angew. Chem. Int. Ed. 50 (2011) 2904.
[4] R. Muhammadpour, A.I. Zad, A. Hagfeldt, G. Boschloo, ChemPhysChem 11 (2010) 2040.
[5] K.D. Benkstien, N. Kopidakis, J. Van de Lagemaat, A.J. Frank, J. Phys. Chem. B 107 (2003) 7759.
[6] K. Zhu, T.B. Vinzant, N.R. Neale, A.J. Frank, Nano Lett. 12 (2007) 3729.
[7] P. Docampo, S. Guldin, U. Steiner, H. Snaith, J. Phys. Chem. Lett. 4 (2013) 698.
[8] J.V. Cab, S.R. Jang, A.F. Halverson, K. Zhu, A.J. Frank, Nano Lett. 14 (2305) (2014) 5.
[9] P.E. De Jongh, E.A. Meulenkamp, D. Vanmackelbergh, J.J. Kelly, J. Phys. Chem. B 104 (2000) 7686.
[10] G.H. Schoenmakers, D. Vanmackelbergh, J.J. Kelly, J. Phys. Chem. 100 (1996) 3215.
[11] A.J. Frank, N. Kopidakis, J.V. De Langemaat, Co-ordination Chem. Rev. 248 (2004) 1165.
[12] R. Mohammadpour, A. Hagfeldt, G. Boschloo, ChemPhysChem 11 (2010) 2140.
[13] B. Roose, H. Pathak, U. Steiner, Chem. Soc. Rev. 44 (2015) 8326.
[14] Y.C. Nah, I. Paramasivam, P. Schmuki, ChemPhysChem 11 (2010) 2698.
[15] S.G. Kumar, L.G. Devi, J. Phys. Chem. A 115 (2011) 13211.
[16] A.E.R. Mohamed, S. Rohani, Energy Environ. Sci. 4 (2011) 1065.
[17] Y. Lai, L. Sun, Y. Chen, H. Zhuang, C. Lin, J.W. Chin, J. Electrochem. Soc. 153 (2006) D123, TiO_2.
[18] M. Mayer, SIMNRA User's Guide, Report IPP 9/113, Max-Planck-Institut für Plasma physik, Garching, Germany, 1997.
[19] M. Yilmaz, B.B. Cirak, S. Aydogan, M.L. Grilli, M. Biber, Superlattices Microstruct. 113 (2017) 310.
[20] R. López, R. Gómez, J. Sol-Gel Sci. Technol. 61 (2012) 1.